Catalysis Today 142 (2009) 78–84

Contents lists available at ScienceDirect

Catalysis Today

journal homepage: www.elsevier.com/locate/cattod

Ni-catalysts obtained from silicate intercalated HTlcs active in the catalytic partial oxidation of methane: Influence of the silicate content

F. Basile [a], P. Benito [a,*], G. Fornasari [a], D. Gazzoli [b], I. Pettiti [b], V. Rosetti [a], A. Vaccari [a]

[a] Dip. Chim. Ind. e dei Mat., Università di Bologna, V.le Risorgimento 4, INSTM U.d.R. Bologna, 40136 Bologna, Italy
[b] Dip. Chimica, Università di Roma "La Sapienza", P.le A. Moro 5, 00185 Roma, Italy

ARTICLE INFO

Article history:
Available online 20 February 2009

Keywords:
Hydrotalcite
Nickel
Silicate
Catalytic partial oxidation
Methane

ABSTRACT

Ni-containing silicate catalysts obtained by decomposition of hydrotalcite-like compounds (HTlcs) were tested in the catalytic partial oxidation (CPO) of methane. The effect of the amount of silicates on the properties and performances of catalysts with different nickel load ($Ni_8Mg_{60}Al_{32}$ and $Ni_2Mg_{66}Al_{32}$) was studied. Catalysts were characterized by X-Ray Diffraction (XRD), X-Ray Photoelectron Spectroscopy (XPS), Temperature Programmed Reduction/Oxidation (TPR/O), H_2 chemisorption, N_2 adsorption/desorption at −196 °C. The amount of silicates determined structural and textural properties of the catalysts forming the forsterite phase after thermal treatment. Increasing the silicate load, the specific surface area (S_{BET}) and the Ni dispersion decreased, but the reducibility of Ni^{2+} species was not modified. Catalytic activity depended on the nickel load and the amount of silicate anions. Catalysts with high Ni content ($Ni_8Mg_{60}Al_{32}$) were active and stable. Catalysts with low Ni load ($Ni_2Mg_{66}Al_{32}$) showed good catalytic performances at the beginning of the tests; however, the samples with large silicate content deactivated by oxidation of Ni^0 particles.

1. Introduction

Catalytic partial oxidation (CPO) of methane, regarded as one of the most promising processes for hydrogen production and gas-to-liquid technologies, particularly in chemical plants of medium size and for microreactors, constitutes an alternative to the steam reforming process [1]. Noble metals are the most active catalysts in the partial oxidation process; however, their high cost and limited availability from the industrial point of view make it necessary to develop alternative catalysts. In this sense, Ni-containing catalysts are widely studied, since they are more economic; however, they show a lower stability than noble metals. Catalyst deactivation can occur by coke formation, sintering or oxidation of the active metal species. For this reason, the development of stable and active Ni-based catalysts is an important topic of research in the CPO process [2]. A well established alternative to catalysts prepared by impregnation is the use of precursors containing the metal ions inside the crystal structure, such as perovskites and hydrotalcite-like compounds [3]. Hydrotalcite-like compounds are lamellar materials with general chemical formulae $[Mg^{2+}_{1-x}Al^{3+}_x(OH)_2](A^{b-})_{x/b}\cdot mH_2O$. A wide variety of compounds have been prepared modifying both the nature of the layers and the interlayer region [4–6]. The advantage of using HTlcs as precursors of catalysts arises from the fact that their thermal activation leads to basic mixed oxides, with relatively large specific surface area, high thermal stability and dispersion of the active species [7]. Since the atoms occupy random positions in the layers of the precursor and the decomposition takes place topotactically, the cations keep their original location in the mixed oxide, thus highly dispersed metallic species in an inert matrix are obtained after reduction. Among HTlcs those intercalated with carbonate are largely used. After calcination at high temperatures MgO- and spinel-type phases were formed, with Ni^{2+} cations well dispersed in the MgO-type phase [8]. On the other hand, together with the catalytic activity and stability, a good mechanical stability of the catalysts is crucial for many technical applications. In the CPO process catalysts are under high mechanical stress because of the pressure and the high space velocity. The mechanical stability of the mixed oxides derived from HTlcs can be improved by using silicates. They are inserted in the structure of the precursor as counter anion in the interlayer region. Conversely to carbonate anions, silicates do not decompose into volatile species when calcinating at high temperatures and they contribute to the catalysts structure [9–11]. In previous works, it has been shown that the introduction of silicates in the structure of the catalysts not only improves the mechanical stability but also the activity and selectivity towards syngas [9], even for low amounts of active phase [10].

* Corresponding author.
E-mail address: pbenito@ms.fci.unibo.it (P. Benito).

0920-5861/$ – see front matter © 2009 Elsevier B.V. All rights reserved.
doi:10.1016/j.cattod.2009.01.013

In this work, the influence of the amount of silicates and the nickel load on the structure and on catalytic performances of catalysts was investigated for Ni-containing catalysts derived from silicate intercalated hydrotalcite structures. Hydrotalcite-like compounds with a molar ratio $M^{2+}/M^{3+} = 68/32$, and variable nickel load, $Ni_8Mg_{60}Al_{32}$ and $Ni_2Mg_{66}Al_{32}$ were prepared by coprecipitation. The compensating anions were either excess amount of silicates (30%, 20%) or stoichiometric amount (where the excess refers to the amount of anion for balancing the charge excess of the brucite-type layers). The catalysts were characterized and tested in the catalytic partial oxidation of methane under different working conditions to study both their activity and stability.

2. Experimental

2.1. Synthesis

Silicate-containing samples were prepared following the coprecipitation method at constant pH. A 0.2 M solution containing the nitrate salts of the cations in the appropriate ratios was slowly added to a solution containing silicates (sodium silicate solution, NaOH (≥10%), SiO_2 (≥27%), Aldrich). The pH was kept constant by NaOH addition (10.5 ± 0.2). The obtained precipitate was kept in suspension under stirring at 60 °C for 45 min, then filtered and washed with distilled water until a Na_2O content lower than 0.02 wt.% was obtained. The precipitate was dried overnight at 60 °C and catalysts were obtained by calcination at 900 °C for 12 h. The precursors were named as: Ni8HT-*x* and Ni2HT-*x* for $Ni_8Mg_{60}Al_{32}$ and $Ni_2Mg_{66}Al_{32}$ series, where *x* stands for the amount of silicate, 30%, 20% and stoich (stoichiometric). Calcined samples were identified by adding "ex" in the label of the precursors, i.e. Ni8exHT-30. Table 1 listed the labels and composition of the catalysts studied.

2.2. Characterization techniques

XRD powder analyses were carried out using a Philips PW1050/81 diffractometer equipped with a graphite monochromator in the diffracted beam and controlled by a PW1710 unit (CuKα-Ni filtered, λ = 0.15418 nm). A 2θ range from 10° to 80° was investigated at a scanning speed of 70° h^{-1}. Temperature Programmed Reduction and Oxidation (TPR/O) analyses were carried out with an H_2/Ar and O_2/N_2 5/95 (v/v) gas mixture respectively (total flow rate 20 mL/min) gas mixture in the 100–950 °C temperature range in a ThermoQuest CE instruments TPDRO 1100. Specific surface area measurements were carried out in a Micromeritics ASAP 2020 instrument. Samples were previously degassed under vacuum and heated up to 250 °C and maintained for 30 min. Chemisorption measurements of H_2 were carried out with a Micromeritics ASAP 2020 instrument using a conventional static method. The metal surface area (S_m, $m^2\ g^{-1}$), dispersion (*D*, %), and metal particle size (*d*, nm) were determined from the H_2 chemisorption data, using a 1/1 H/Ni titration stoichiometry. The samples were reduced for 2 h at 750 °C in pure H_2 and cooled to room temperature under vacuum. The hydrogen adsorption isotherm was established at 35 °C. After evacuation at room temperature, a second H_2 isotherm was performed. By taking the differences between the isotherms, the amount of irreversibly adsorbed hydrogen was determined. The gas uptake of metallic phase was obtained by extrapolating to zero pressure.

XPS spectra were collected by a Leybold-Heraeus LHS10 spectrometer operating in FAT mode (50 eV pass energy), using a twin AlKα (12 kV/20 mA) and MgKα (10 kV/20 mA) anode at a pressure better than 10^{-9} Torr. The samples, reduced to fine powders, were manually pressed onto a double side tape attached to the sample rod. In situ treatments in a flowing H_2/N_2 mixture (H_2 10%, 6 mL/min) at 450 °C for 4 h were carried out in a chamber connected to the preparation chamber on the sample reduced in the catalytic apparatus (see below). The treatment temperature refers to the effective sample temperature monitored by a thermocouple contacting the sample surface. After being cooled gradually to room temperature in the H_2/N_2 stream the sample was transferred in vacuo to the preparation chamber and then pushed into the analysis chamber for spectra collection.

The Ni2p, C1s, O1s, Si2s, Al2s, Si2p, Mg2s, Al2p and Mg2p regions were sequentially acquired. Binding energies (BE) were referenced to C1s at 285.0 eV and measured with an accuracy of ± 0.2 eV. Data analysis involved smoothing, non-linear Shirley-type background subtraction, curve-fitting and peak areas by integration of the appropriate peak by Esca Tools 4.2 software (Surface Interface Inc., Mountain View, California). Because Al2p peak overlaps with the Ni3p signal, as well as Al2s with Ni3s, their contributions were determined by curve-fitting. Changes in the Ni2p signal shape on reduced samples were analysed by curve-fitting procedures with Ni2p doublets endowed with fixed spectroscopic parameters ($Ni2p_{3/2}$–$2p_{1/2}$ spin-orbit separation, 17.2 eV and intensity ratio *R* = 0.50) but using variable position, full width at half maximum (FWHM) and intensities. Surface composition was obtained from peak area ratios by using the elemental sensitivity factors method [12].

2.3. Catalytic tests

Catalytic tests were carried out in a quartz reactor (i.d. 8 mm) filled with 0.5 g of catalyst with particle size between 0.60 and 0.42 mm to avoid pressure drop giving a bed length of about 2 cm. Catalysts were reduced in situ at 750 °C in an equimolar H_2/N_2 mixture (7 L/h) The reactor was inserted in an electric oven, where several gas mixtures were fed at two different temperatures: (i) $CH_4/O_2/He = 2/1/20$, *T*(oven) = 500 and 750 °C, τ = 65 ms; (ii) $CH_4/O_2/He = 2/1/4$, *T*(oven) = 750 °C, τ = 65 ms; (iii) $CH_4/O_2/He = 2/1/1$, *T*(oven) = 750 °C, τ = 112 ms; (iv) $CH_4/O_2/He = 4/2/2$, *T*(oven) = 750 °C, τ = 52 ms (τ being calculated as weight of catalyst on total flow). The gas phase temperature was measured by a moveable chromel–alumel thermocouple sliding in a quartz wire inside the catalytic bed. The reaction products were analysed on-line after water condensation by two gas chromatographs equipped with HWD and Carbosieve SII columns, using He as the carrier gas for the analysis of CH_4, O_2, CO and CO_2 and N_2 for the H_2 analysis. The oxygen conversion was complete in the whole series of the catalytic tests and the carbon balance was always between 98% and 102%.

Table 1
Summary of the catalysts prepared and tested in the CPO of methane.

Sample	Atomic ratio	Silicate content	Ni (wt.%)
Ni8exHT-30	$Ni_8Mg_{60}Al_{32}$	30% Excess	7.96
Ni8exHT-20	$Ni_8Mg_{60}Al_{32}$	20% Excess	8.09
Ni8exHT-stoich	$Ni_8Mg_{60}Al_{32}$	Stoichiometric	8.37
Ni2exHT-30	$Ni_2Mg_{66}Al_{32}$	30% Excess	2.06
Ni2exHT-20	$Ni_2Mg_{66}Al_{32}$	20% Excess	2.10
Ni2exHT-stoich	$Ni_2Mg_{66}Al_{32}$	Stoichiometric	2.17

3. Results and discussion

3.1. Characterization of the catalysts

XRD patterns of the precursors obtained by coprecipitation were characteristic of poorly crystallized HTlcs with silicate anions placed in the interlayer forming polysilicates [11–13]. However, some carbonate anions, coming from CO_2 in the atmosphere, could also be in the interlayer region as contaminant species because of

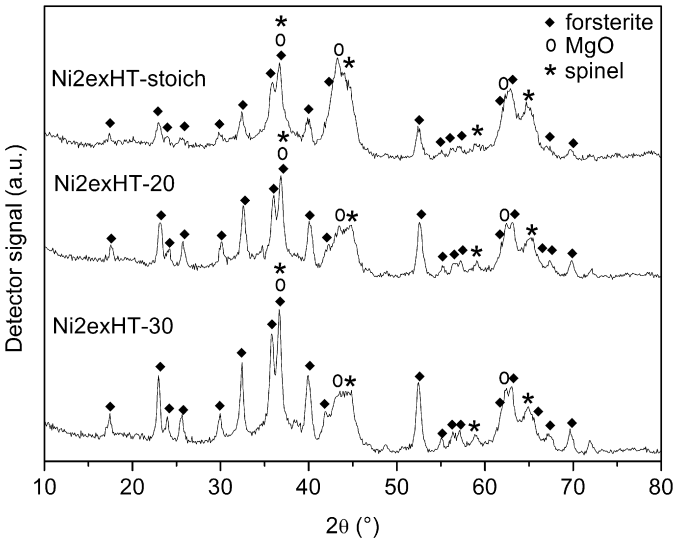

Fig. 1. XRD of Ni2exHT-catalysts with different silicate content calcined at 900 °C.

the high affinity of HTlcs to them. Neither the amount of silicate nor the nickel load greatly altered the structure of the HTlcs.

After thermal treatment, similar diffraction patterns were recorded for all the catalysts, regardless of the composition of the precursor, Fig. 1. Three crystalline phases were identified [9]: forsterite (Mg_2SiO_4), rock-salt (MgO) and a spinel-type ($MgAl_2O_4$) phase. However, the presence of some amorphous silica could not be ruled out. Increasing the silicate content diffraction lines due to the forsterite phase gained intensity and became narrower. Unfortunately, the overlapping of the reflections of the rock-salt and spinel phases to those of the Mg_2SiO_4 phase made rather complex the study of the patterns. However, it was clearly seen that decreasing the silicate load, the reflections due to the MgO phase grew in intensity as expected, because Mg^{2+} cations were not employed to form the forsterite phase. Nevertheless, no modification of the peaks attributed to the spinel phase was observed. Moreover, a comparison among patterns of the samples with different nickel load, Ni8exHT-*x* and Ni2exHT-*x*, particularly regarding the intensity of forsterite and MgO highest peaks revealed that the amount of segregated MgO-type phase increased with Ni content.

The XPS analysis has been applied to study the surface properties of Ni8exHT-*x* and Ni2exHT-*x* samples. The Mg2p BE value was found at 50.4 ± 0.2 eV and the Al2p at 74.4 ± 0.2 eV in all the samples, in agreement with literature data [14]. Si2p was at 102.3 ± 0.2 eV as found for forsterite (Mg_2SiO_4) [15]. $Ni2p_{3/2}$ was at 856. 6 ± 0.2 eV (FWHM about 2.8–3.2 eV) with a shake up at about 6.2 eV higher BE, consistent with the presence of Ni^{2+} in $MgAl_2O_4$-like structures [16,17]. The O1s feature was asymmetric and resolved with two components at about 531.3 eV and 532.5 eV, representing two different kinds of surface oxygen species. The component at about 531.3 eV is characteristic of lattice oxygen in aluminium compounds whereas that at 532.5 eV agrees with the values found for silicon-containing compounds [18]. The relative abundance of these two oxygen species varied in the range 70–80% (low BE component) and 20–30% (high BE component), respectively. The surface composition was evaluated from the Ni2p/Mg2p (Ni/Mg), Ni2p/Al2p (Ni/Al), Mg2p/Al2p (Mg/Al) and Mg2p/Si2p (Mg/Si) atomic ratios as described in Section 2. The XPS data proved that the surface concentrations of nickel and aluminium were higher than those expected for the stoichiometric values, revealing a higher mobility of nickel and aluminium species towards the surface, Table 2. Comparing the bulk composition with the XPS-derived surface composition for Ni2exHT-stoich and Ni8exHT-stoich samples, the Ni2exHT-stoich sample showed a surface enrichment in nickel and aluminium, whereas in the Ni8exHT-stoich sample similar bulk and surface concentration were found for Ni, with a surface enrichment in Al. Both samples had, however, a lower silicon content. An increase in Ni and Al surface content was apparent for the Ni2exHT-20 and Ni8exHT-20 samples (Table 2), whereas the surface silicon content decreased with nickel content. A similar trend was found for the Ni2exHT-30 and Ni8exHT-30, with Ni and Al surface enrichment in the Ni2exHT-30 sample larger than in the Ni8exHT-30 sample and silicon content close to that in the bulk.

The amount of silicate influenced the specific surface areas of catalysts, the larger the silicate load the lower the S_{BET} values, Table 3. This behaviour could be explained taking into account that an increase in silicon content parallels a decrease in carbonate anions. At low silicate content, the carbonate anions, present in the HTlc as contaminant species, could be more abundant with a consequent increase of the specific surface area during the thermal decomposition due to the cratering mechanism, produced by the evolution of CO_2 and H_2O gases [19]. On the other hand, the decreased surface area at increasing silicate content could be also related to the formation of a large amount of well crystallized forsterite phase leading to lower sample porosity.

Active species in the CPO process are Ni metal species, thus it was useful to study whether the reducibility of Ni^{2+} species was influenced by the silicate content. Temperature Programmed Reduction (TPR) profiles of all the Ni8exHT-*x* and Ni2exHT-*x* catalysts showed single H_2 consumption curves with maxima at high temperatures (Fig. 2), characteristic of Ni^{2+} species well stabilized in the matrix against reduction. Although a single peak was observed, TPR profiles could represent the convolution of several H_2 consumption peaks, correspondent to the reduction of different species taking place at close temperatures. Ni^{2+} cations could be inserted in MgO to form the $Ni_xMg_{1-x}O$ solid solution or in the spinel phase to form $Ni_xMg_{1-x}Al_2O_4$ or in both, in agreement with XPS results. The position of the maxima was not related to the amount of silicates, but it slightly depended on the nickel load. The shift of the maxima towards higher

Table 2
Bulk and XPS-derived surface composition for Ni8exHT and Ni2exHT samples.

Sample	Bulk composition				Surface composition			
	Ni/Mg	Ni/Al	Mg/Al	Mg/Si	Ni/Mg	Ni/Al	Mg/Al	Mg/Si
Ni8exHT-30	0.133	0.250	1.875	2.884	0.165	0.265	1.506	3.560
Ni8exHT-20	0.133	0.250	1.875	3.125	0.258	0.349	1.347	3.407
Ni8exHT-20 red					0.091	0.128	1.82	3.18
Ni8exHT-stoich	0.133	0.250	1.875	3.750	0.135	0.197	1.470	4.450
Ni2exHT-30	0.030	0.062	2.062	3.173	0.052	0.073	2.030	3.660
Ni2exHT-20	0.030	0.062	2.062	3.437	0.066	0.102	1.540	2.840
Ni2exHT-20 red					0.031	0.064	2.04	3.6
Ni2exHT-stoich	0.030	0.062	2.062	4.125	0.045	0.075	1.658	5.350

Table 3
S_{BET} of the fresh and used catalysts and metal dispersion, metallic surface area and apparent crystallite sizes obtained by H_2 chemisorption.

Sample	S_{BET} fresh ($m^2\ g^{-1}$)	S_{BET} used ($m^2\ g^{-1}$)	Metal dispersion (%)	Metallic surface area ($m^2\ g^{-1}$ metal)	Apparent crystallite size (nm)
Ni8exHT-30	73	72	2.70	18	37
Ni8exHT-20	96	95	5.08	34	20
Ni8exHT-stoich	113	103	5.31	36	19
Ni2exHT-30	108	85	2.10	14	48
Ni2exHT-20	112	91	3.55	24	29
Ni2exHT-stoich	121	116	0.81	5	125

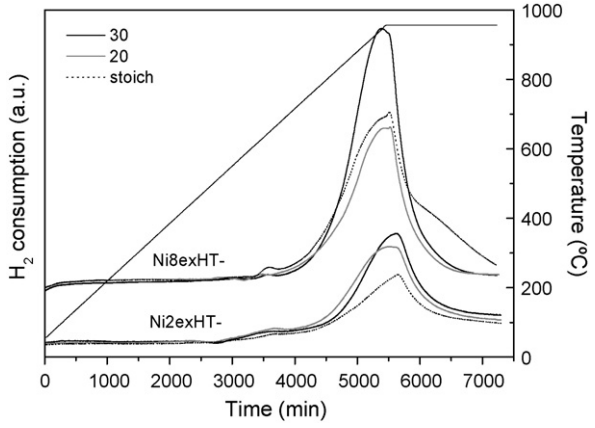

Fig. 2. TPR profiles of catalysts with different nickel and silicate content (Ni8exHT- and Ni2exHT-catalysts).

temperatures observed when the nickel load decreased could be the consequence of a better dispersion of the species within the matrix hindering its reduction. The amount of hydrogen consumed was calculated from the area of the TPR peaks and related to the concentration of reducible Ni^{2+} cations. Hydrogen consumption for Ni8exHT-*x* and Ni2exHT-*x* catalysts was lower than that required for the stoichiometric reduction of Ni^{2+} to Ni^0. The results indicated that about a 60% of Ni^{2+} cations were effectively reduced during the analyses.

In order to further investigate whether Ni^{2+} was fully reduced to the metallic state, the XPS characterization was performed on two representative samples (Ni2exHT-20 red and Ni8exHT-20 red) reduced in situ in the catalytic reactor, following the same pre-treatment of those submitted to catalytic tests. Reduction in H_2 at 750 °C for 12 h of Ni8exHT-20 and Ni2exHT-20 samples, caused substantial changes in the Ni2p feature whereas no changes either in BE or peak shape of all the other elements were observed. The Ni2p peaks were broader than those in calcined samples and composite because of the presence of components at 853.1 eV and at 856.7 eV ascribable to Ni(0) and Ni(II), respectively. To determine whether the presence of Ni(II) species is due to incomplete reduction or partial oxidation owing to the exposure of samples to air, in situ treatment in H_2 at 750 °C for 4 h were performed. The Ni2p feature was still complex and curve-fitting gave components at 852.8 eV and at 856.8 eV, each carrying 70% and 30% of the total intensity. The two components are assigned to Ni(0) and Ni(II), respectively, indicative of the incomplete reduction of Ni^{2+}. In addition, the strong decrease in the Ni2p peak intensity after H_2 treatment at 750 °C, about 50%, results in a surface concentration close to that of the bulk, indicating that heating caused an agglomeration of the surface species, Table 2.

After the reduction step in the TPR, the samples were submitted to a cycle of Temperature Programmed Oxidation (TPO). TPO profiles exhibited broad peaks starting at rather low temperature, about 175 °C, Fig. 3. The oxidation temperature depended either on the amount of silicates or on the nickel load. The complex shape of the peaks suggested overlapping steps, possibly associated with the re-oxidation of different Ni species [20]. Decreasing the nickel load, led to a considerable shift of the maxima towards lower temperatures, and this could be explained with the formation of small metallic particles that were more easily oxidized [21]. Regarding the influence of the silicate content, no significant differences were found for Ni8exHT-catalysts with a 30% and a 20% in excess but a decrease in the oxidation temperature was observed for the Ni8exHT-stoich catalyst. On the other hand, for Ni2exHT-samples, the lower the silicates amount, the higher the stability against the oxidation.

Finally, the study of the dispersion of Ni metal in the catalysts was important, since it generally influences the catalytic activity and selectivity. Results obtained from H_2 chemisorption are summarized in Table 3. Dispersion, metallic surface area and metallic apparent crystal size depended on both the Ni content and the silicate amount. Concerning the effect of the nickel content, the higher the Ni load the larger the dispersion values. This behaviour was the opposite of that expected, because the high nickel load would have led to large particles with low dispersion degree. Nevertheless, the values could be related to an incomplete reduction of nickel cations during the catalyst activation in agreement with TPR and XPS results of reduced samples and in line with literature findings [22,23]. Regarding the amount of silicates, for Ni8exHT-catalysts, the Ni dispersion decreased increasing silicate content, slightly for the Ni8exHT-20 sample and markedly for the Ni8exHT-30 sample. The values reported in Table 3 could be explained taking into account that the amount of silicates influenced the relative ratio of forsterite/MgO/spinel phases and that the specific surface area of the samples also depended on the silicate content. For Ni2exHT-series, the same trend was observed for samples with a 30% and a 20% excess of silicates. Conversely, the stoichiometric catalyst Ni2exHT-stoich, showed no appreciable Ni dispersion, although the amount of MgO phase was maximized in

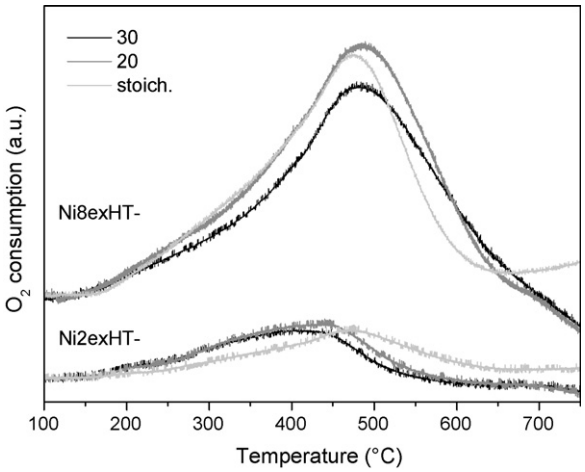

Fig. 3. TPO profiles of Ni8exHT- and Ni2exHT-catalysts with different silicate content (30%, 20% and stoichiometric amount).

Table 4
Maximum reaction temperature (T_{max}) and outlet temperature (T_{out}) of the gas phase measured by the thermocouple for all the catalysts.

CH_4/O_2/He (v/v)	2/1/20		2/1/20		2/1/4		2/1/1		4/2/2		2/1/20	
T_{oven} (°C)	500		750		750		750		750		500	
Sample	T_{out}	T_{max}	T_{out}	T_{max}	T_{out}	T_{max}	T_{out}	T_{max}	T_{out}	T_{max}	T_{out}	T_{max}
Ni8exHT-30	525	584	747	767	756	814	753	823	778	865	515	581
Ni8exHT-20	520	583	746	771	757	824	760	832	780	875	513	579
Ni8exHT-stoich	526	589	748	776	756	829	756	829	775	891	515	595
Ni2 exHT-30	520	576	750	786	752	862	753	887	755	910	542	572
Ni2 exHT-20	543	579	745	775	753	863	756	910	759	948	558	584
Ni2 exHT-stoich	530	578	747	772	768	829	753	840	752	899	540	565

this solid. It should be noticed that this catalyst showed a good catalytic performance (see below). Ni dispersion could be explained with a strong metal–support interaction [24]. Ni^{2+} embedded in the MgO structure was not easily available to the hydrogen [25]. Apparent crystallite sizes of Ni^0 particles calculated by H_2 chemisorption ranged from 37 to 19 nm for Ni8exHT-catalysts and from 125 to 29 nm for Ni2exHT-catalysts.

3.2. Catalytic tests

The effect of the catalyst composition (nickel load and amount of silicates) on the catalytic performances was examined by feeding CH_4/O_2/He gas mixture with different volumetric ratios at 500 and 750 °C. Tests at 500 °C and in diluted conditions (2/1/20, v/v CH_4/O_2/He), where the amount of heat evolved because of the exothermicity decreased and the thermal conductivity of the gas increased, highlighted differences among catalysts. On the other hand, when the oven temperature was set at 750 °C and more concentrated gas mixtures were fed, reaction conditions were closer to industrial ones and they were useful to test the catalyst stability. After tests at high temperature, the catalysts were further tested using the same conditions as in the first test to study whether some deactivation process had taken place with increasing the time-on-stream. The results showed that catalytic performances differed depending on the nickel load and the amount of silicate anions.

The gas phase temperature was also measured with a chromel–alumel thermocouple placed inside the catalyst bed. Catalytic tests were not performed in isothermal conditions, the temperature of the catalytic bed varied following the exothermicity and/or endothermicity of the reactions occurring along the bed so an axial temperature gradient was observed. A high temperature spot was observed at the beginning of the catalytic bed due to the oxidation of methane (total or partial), whereas at the end of the bed the gas temperature decreased due to reforming reactions and a value close to that of the oven temperature was measured. The maximum (T_{max}) as well as the outlet temperature (T_{out}) were taken, Table 4. Although, the temperature of the gas was not similar to the real surface catalyst temperature [26], it gave an idea about the reactions taking place in the different parts of the catalyst bed. The results summarized in Table 4 indicated that the difference between T_{max} and T_{out} changed with the oven temperature, gas mixture concentration and contact time. Moreover, some differences were observed changing the chemical composition of the catalyst.

Catalysts with high Ni content, Ni8exHT-*x*, exhibited good catalytic performances whatever the fed gas mixture and the temperature set. Methane conversion and selectivities in CO and in H_2 were shown in Figs. 4 and 5. The catalytic activity at 500 °C was high, with methane conversion in the range from 56% to 61% depending on the amount of silicates. The high H_2/CO ratios were related to the contribution of the water gas shift (WGS) reaction. The best catalytic performances in terms of methane conversion and selectivity in syngas were achieved with the sample with a 20% excess of silicates. At 750 °C and feeding the most diluted mixture (2/1/20, v/v) the differences were smoothed, because at low pressures and high temperature the thermodynamic equilibrium was easily reached, yielding conversion of methane around 97% and selectivity in CO (S_{CO}) and H_2 (S_{H_2}) close to 100%. By concentrating the gas mixture (2/1/4 and 2/1/1, v/v) methane conversion decreased and selectivity in CO was higher than in H_2. In this case, the high S_{CO} was attributed to the reverse water gas shift reaction. The increase of the flow rate in a factor of two (4/2/2, v/v) caused a slight increase in the methane conversion, since the decrease of the residence time was balanced by the increase of the catalyst surface temperature and thus of the gas phase temperature as observed in Table 4. Although, all catalysts were active approaching the thermodynamic equilibrium, Ni8exHT-20 sample showed the best catalytic performances under these reaction conditions. Finally, setting again the initial conditions, methane conversion and selectivity to CO and H_2 were higher than those

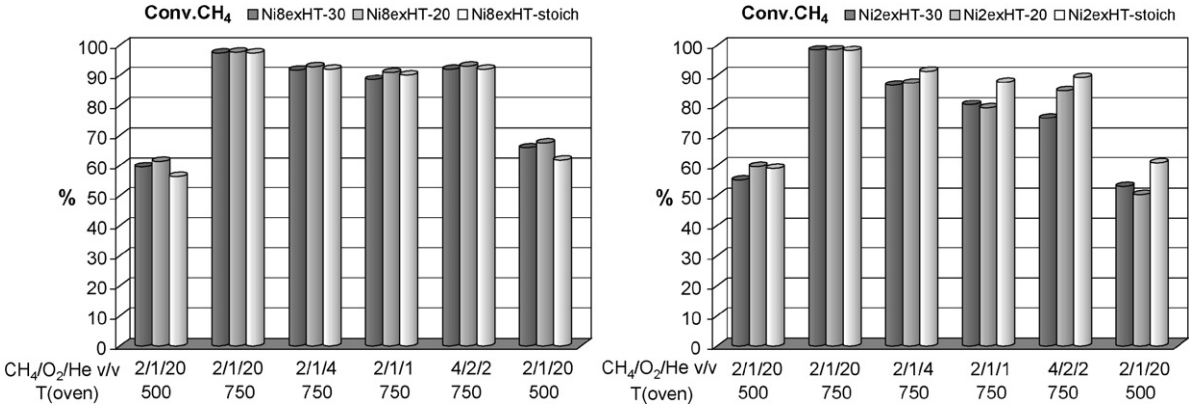

Fig. 4. Conversion of CH_4 of Ni8exHT- (left) and Ni2exHT- (right) catalysts with different silicate content under all the reaction conditions.

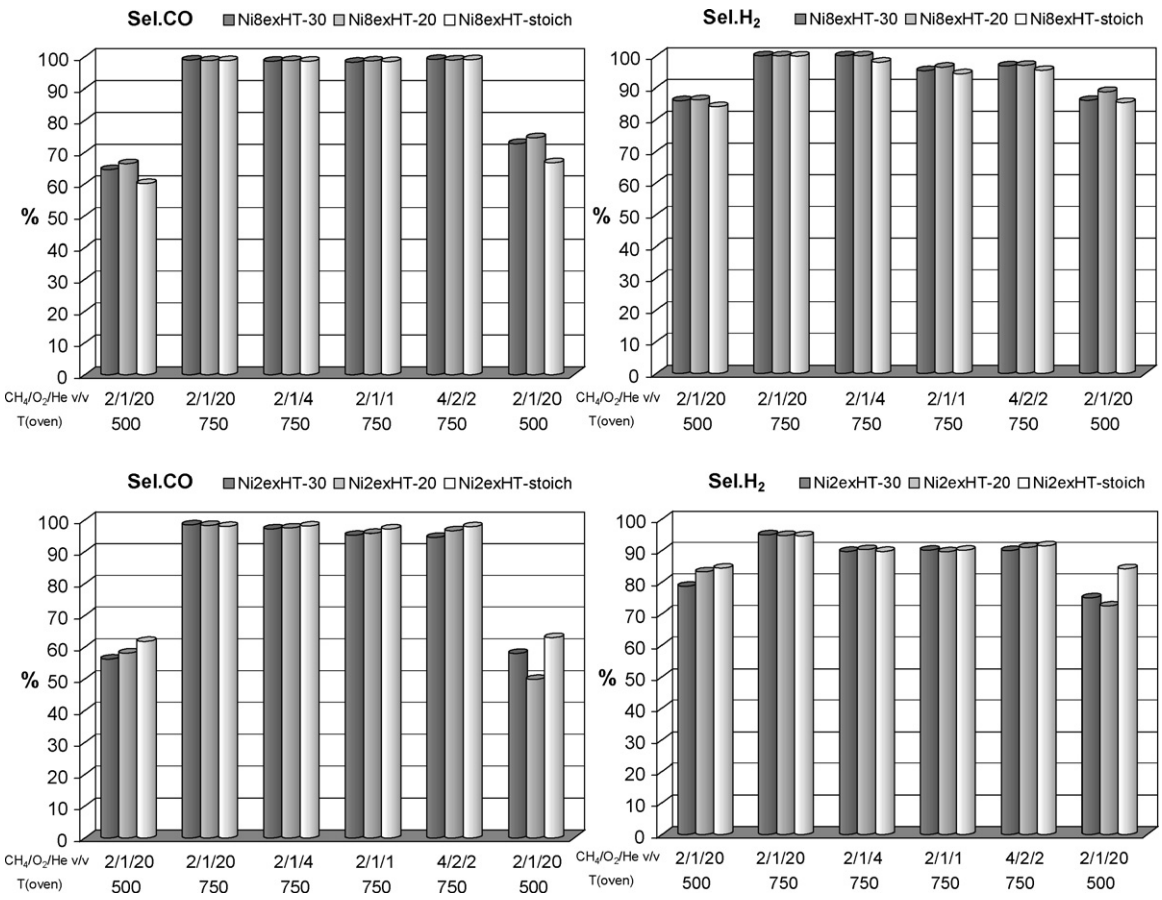

Fig. 5. Selectivity in CO and H_2 of Ni8exHT- (above) and Ni2exHT- (below) catalysts with different silicate content.

obtained in the initial test for all catalysts, in the order: Ni8exHT-20 > Ni8exHT-stoich > Ni8exHT-30. As shown in the TPR, XPS analysis and by H_2 chemisorption, it seemed that the reduction pre-treatment was not effective for the complete reduction of Ni^{2+} species. During catalytic tests an additional activation should have occurred [24,27,28], resulting in an increased activity. Finally, the different experimental conditions should also be considered, for the initial conditions after start-up, the mixture was fed at 500 °C after a He stream, whereas the return was carried out by lowering the temperature and diluting the gas in reaction stream from hard conditions, high reduction atmosphere, keeping a larger amount of Ni species in the metallic state [10].

Ni2exHT-*x* catalysts, during the tests performed at 500 °C and feeding the 2/1/20 (v/v) gas mixture, exhibited methane conversions and syngas selectivities only slightly lower than those observed for Ni8exHT-catalysts, despite the considerable decrease of the active phase. Although the differences were not very remarkable, the catalyst with 20% excess of silicates was slightly more active.

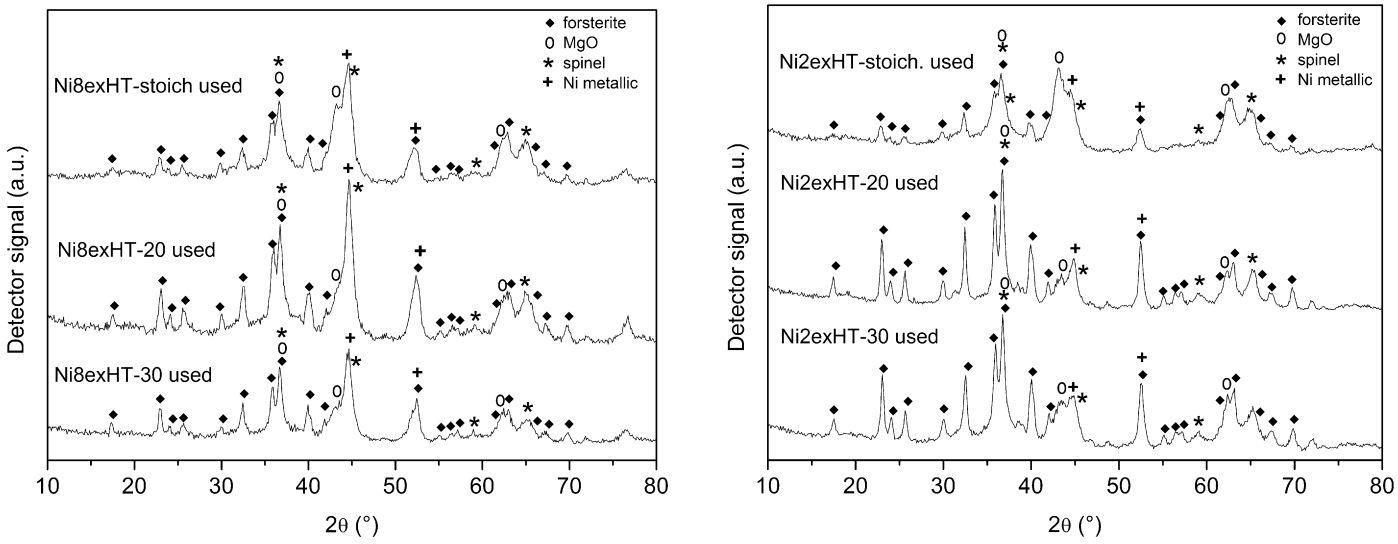

Fig. 6. XRD patterns of used Ni8exHT- (left) and Ni2exHT-catalysts (right) with different silicate content.

Increasing the oven temperature (but keeping the same gas feed) all the catalysts were active reaching the thermodynamic equilibrium. However, under more drastic conditions the low nickel load led to a decrease of the methane conversion for catalysts increasing silicate load. A deactivation of the catalysts took place, probably due to the oxidation of Ni metal particles, being higher for the Ni2exHT-30 sample. It should be remarked that lower CO and H_2 selectivity values were also obtained for catalysts with 20% and 30% in excess of silicates. These lower values could be related to a contribution of the total oxidation of methane occurring over oxidized nickel particles [29]. The evidence that the measured T_{max} for these catalysts were higher than those recorded for Ni8exHT-*x* and Ni2exHT-stoich ones supported this idea, Table 4. It could be also thought that the process was not entirely heterogeneous for Ni2exHT-30 and Ni2exHT-20 catalysts. Finally, when the initial conditions were set again, similarly to Ni8exHT-*x* samples, the Ni2exHT-stoich catalyst was activated, nevertheless catalysts with a 30% and 20% excess of silicates led to lower conversion values.

3.3. Used catalysts

The characterization of used catalysts by XRD and N_2 adsorption/desorption at −196 °C gave additional information about catalytic performances and deactivation processes. Diffraction patterns of used Ni8exHT-*x* samples were quite similar to those recorded for the fresh samples Fig. 6 vs Fig. 1 and no variation of the specific surface area was measured, Table 2. These facts could indicate that no sintering took place with increasing time-on-stream. In the diffraction patterns of used catalysts reflection lines due to the metallic nickel were still present. Although the patterns were very complex, it could be observed that the most intense line due to Ni^0 at around $2\theta = 44^\circ$ was higher for the Ni8exHT-20 sample, the catalyst showing the best performances. This feature could be attributed to the sintering of the metallic particles; however, since neither reduction in the catalytic performances nor lowering of the specific surface area was observed, the increase in intensity could be related to a further reduction occurring under reaction conditions. Finally, it should be remarked the high stability of the forsterite phase, wherein the presence of isolated SiO_4^{4-} units (linked by Mg^{2+}) inhibited its decomposition and vaporisation [30].

XRD patterns of used Ni2exHT-*x* catalysts showed narrower diffraction lines than fresh catalysts, Fig. 6 vs Fig. 1. However, the sintering process did not take place massively, since only a slight decrease of the surface area occurred, Table 2. Moreover, no carbon formation was detected which could have been responsible for the deactivation of the catalysts previously described. Nevertheless, no intense reflections due to metallic nickel were observed, probably due to the re-oxidation of metal particles (although, the decrease of the intensity due to the low nickel load could not be ruled out). After tests, the catalytic bed did not appear uniform: three fractions with different colour were observed pointing to a change in the phase composition with the axial direction of the gas stream as previously observed [8]. The first part was green, like the fresh catalyst before the reduction treatment due to NiO; in the middle the catalytic bed was dark greenish whereas the tail remained gray with time-on-stream. So it can be concluded that for Ni2exHT-*x* catalysts regardless the small amount of surface Ni metal species, they can efficiently activate the molecule of methane under initial conditions. However, when the gas mixture was concentrated the decomposition rate of methane over the metallic nickel particles was low and the remaining oxygen reacted with the Ni^0 crystallites particularly for Ni2exHT-30 and Ni2exHT-20 samples; the oxidized fraction increased with the sequence 20% > 30%, and no oxidation was observed for Ni2exHT-stoich. This behaviour agreed with TPO profiles wherein it was shown that the oxidation of reduced Ni2exHT-*x* catalysts took place at lower temperatures.

4. Conclusions

Ni-containing catalysts obtained from hydrotalcite-like compounds (HTlcs) intercalated with silicate anions were prepared to develop active and stable catalysts for the catalytic partial oxidation (CPO) of methane as an alternative to the conventional catalysts obtained intercalating carbonates. The results showed that Ni catalysts obtained by decomposition of HTlcs intercalated by silicate were a good alternative to the conventional carbonate intercalated compounds. Modifying the amount of silicates allowed the tailoring of the structural and textural properties of the catalysts, and then of their catalytic performances. Catalytic results have shown that Ni8exHT-*x* catalysts were stable with increasing the time-on-stream. Reducing the amount of active phase, the best results were achieved using the sample with a lower amount of silicates (stoichiometric). For this catalyst, the amount of magnesium available to form the MgO phase increased, thus a larger amount of Ni^{2+} species could be involved in the solid solution improving the catalyst stability.

Acknowledgement

The financial support from MIUR (Rome) is gratefully acknowledged.

References

[1] A.P.E. York, T.-C. Xiao, M.L.H. Green, J.B. Claridge, Catal. Rev.-Sci. Eng. 49 (2007) 511.
[2] R.M. Navarro, M.A. Peña, J.L.G. Fierro, Chem. Rev. 107 (2007) 3952.
[3] K. Takehira, Catal. Surv. Japan 6 (2002) 19.
[4] F. Cavani, F. Trifirò, A. Vaccari, Catal. Today 11 (1991) 173.
[5] V. Rives (Ed.), Layered Double Hydroxides: Present and Future, Nova Science Publishers, New York, 2001.
[6] X. Duan, D.G. Evans, Structure and Bonding, "Layered Double Hydroxide", Vol. 119, 2006.
[7] S. Albertazzi, F. Basile, A. Vaccari, in: F. Wypych (Ed.), Catalytic Properties of Layered Double Hydroxides, Clay Surfaces: Fundamentals and Applications, Elsevier, Amsterdam, 2004, p. 497.
[8] F. Basile, L. Basini, M. D'Amore, G. Fornasari, A. Guarinoni, D. Matteuzzi, G. Del Piero, F. Trifirò, A. Vaccari, J. Catal. 173 (1998) 247.
[9] P. Arpentinier, F. Basile, P. Del Gallo, G. Fornasari, D. Gary, V. Rosetti, A. Vaccari, Catal. Today 99 (2005) 99.
[10] P. Arpentinier, F. Basile, P. del Gallo, G. Fornasari, D. Gary, V. Rosetti, A. Vaccari, Catal. Today 117 (2006) 462.
[11] S. Albertazzi, F. Basile, P. Benito, P. Del Gallo, G. Fornasari, D. Gary, V. Rosetti, A. Vaccari, Catal. Today 128 (2007) 258.
[12] C.D. Wagner, E.L. Davis, M.V. Zeller, J.A. Taylor, R.H. Raymond, L.H. Gale, Surf. Interface Anal. 3 (1981) 211.
[13] C. Dèpege, F.Z. El Metoui, C. Forano, A. de Roy, J. Dupuis, J.P. Besse, Chem. Mater. 8 (1996) 952.
[14] A.H. Padsmari, A. Venugopal, V. Durga Kumari, K.S. Rama Rao, P. Kanta Rao, J. Mol. Catal. A: Chem. 188 (2002) 225.
[15] K. Okada, Y. Kameshima, A. Yasumori, J. Am. Ceram. Soc. 83 (1998) 1970.
[16] S. Velu, K. Suzuki, M. Vijayara, S. Barman, C.S. Gopinath, Appl. Catal. B: Environ. 55 (2005) 287.
[17] A.P. Grosvenor, M.C. Biesinger, R. At, C. Smart, N.S. McIntyre, Surf. Sci. 600 (2006) 1771.
[18] V. Dimitrov, T. Komatsu, J. Solid State Chem. 163 (2002) 100.
[19] W.T. Reichle, Solid State Ionics 22 (1986) 135.
[20] R. Villa, C. Cristiani, G. Groppi, L. Lietti, P. Forzatti, U. Cornaro, S. Rossini, J. Mol. Catal. A: Chem. 204–205 (2003) 637.
[21] W.H. Hangue, J.R. Katzor, J. Catal. 32 (1974) 166.
[22] K. Nagaoka, A. Jentys, J.A. Lercher, J. Catal. 229 (2005) 185.
[23] T. Miyata, M. Shiraga, D. Li, I. Atabe, T. Shishido, Y. Oumi, T. Sano, K. Takehira, Catal. Commun. 8 (2007) 447.
[24] J.H. Jun, T.-S. Lee, T.H. Lim, S.L. Nam, S.-A. Hong, K.J. Yoon, J. Catal. 221 (2004) 178.
[25] A. Olafsen, C. Daniel, Y. Schuurman, L.B. Raberg, U. Olsbye, C. Mirodatos, Catal. Today 115 (2006) 179.
[26] F. Basile, G. Fornasari, F. Trifirò, A. Vaccari, Catal. Today 64 (2001) 21–30.
[27] K. Sato, S. Fujita, K. Suzuki, T. Mori, Catal. Commun. 8 (2007) 1735.
[28] F. van Looij, J.W. Geus, J. Catal. 168 (1997) 154.
[29] X.Z. Zhang, C.S.-M. Lee, D.O. Hayward, D.M.P. Mingos, Catal. Today 105 (2005) 283.
[30] J. Wang, A.M. Davis, R.N. Clayton, A. Hashimoto, Geochem. Cosmochim. Acta 63 (1999) 953.